

RSC Advances



This is an *Accepted Manuscript*, which has been through the Royal Society of Chemistry peer review process and has been accepted for publication.

Accepted Manuscripts are published online shortly after acceptance, before technical editing, formatting and proof reading. Using this free service, authors can make their results available to the community, in citable form, before we publish the edited article. This *Accepted Manuscript* will be replaced by the edited, formatted and paginated article as soon as this is available.

You can find more information about *Accepted Manuscripts* in the [Information for Authors](#).

Please note that technical editing may introduce minor changes to the text and/or graphics, which may alter content. The journal's standard [Terms & Conditions](#) and the [Ethical guidelines](#) still apply. In no event shall the Royal Society of Chemistry be held responsible for any errors or omissions in this *Accepted Manuscript* or any consequences arising from the use of any information it contains.

Cite this: DOI: 10.1039/c0xx00000x

www.rsc.org/xxxxxx

FULL PAPER

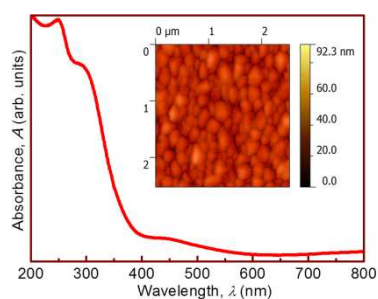
Visible-light photocatalytic activity of nitrogen-doped NiTiO₃ thin film prepared by co-sputtering process

Jagadeesh Babu Bellam^a, Marco Alejandro Ruiz-Preciado^{a,b}, Mathieu Edely^a, Jacek Szade^c, Alain Jouanneaux^a and Abdel Hadi Kassiba^{a*}

⁵ Received (in XXX, XXX) Xth XXXXXXXXX 20XX, Accepted Xth XXXXXXXXX 20XX

DOI: 10.1039/b000000x

NiTiO₃ thin films grown using co-sputtering process exhibited define structural, morphological and optical characteristics, which showed enhanced visible light photocatalytic activity.



10

RSC Advances Accepted Manuscript

Cite this: DOI: 10.1039/c0xx00000x

www.rsc.org/xxxxxx

FULL PAPER

Visible-light photocatalytic activity of nitrogen-doped NiTiO₃ thin film prepared by co-sputtering process

Jagadeesh Babu Bellam^a, Marco Alejandro Ruiz-Preciado^{a,b}, Mathieu Edely^a, Jacek Szade^c, Alain Jouanneaux^a and Abdel Hadi Kassiba^{a*}

5 Received (in XXX, XXX) Xth XXXXXXXXXX 20XX, Accepted Xth XXXXXXXXXX 20XX

DOI: 10.1039/b000000x

Nickel titanate (NiTiO₃) thin films were grown by radio frequency magnetron co-sputtering process using metal (Ni and Ti) targets on fused quartz substrates at a substrate temperature of 400 °C. Annealing of as-deposited (amorphous) films were performed at 1100 °C for 2 hours to realize stable crystalline phase.

10 Effect of Ti target power (200 and 250 W) and nitrogen doping on structural, morphological and optical properties of post-annealed NiTiO₃ thin films were investigated besides photocatalytic activity under visible light irradiation. X-ray diffraction measurement on the films revealed pure ilmenite phase at 250 W Ti power. Preferential orientation changed from [104] to [110] as Ti power increased from 200 to 250 W. Raman studies on NiTiO₃ thin films showed almost all the active modes (5A_g + 5E_g) of a crystalline
15 structure. Two different microstructures were observed by scanning electron microscopy, films showed rounded (250 nm) grains at 200 W Ti target power while facets forms (500 nm) develop in the films deposited at 250 W. Chemical bonding and valence states of the involved ions such as Ni 2p, Ti 2p and O 1s were investigated by X-ray photoelectron spectroscopy. Nitrogen doping modifies the rms roughness from 12 nm to 17 nm as demonstrated on 200W grown films and contributes also to modify the indirect
20 optical band gap from 2.50 to 2.43 eV in films obtained at 250 W Ti target power. As a crucial role of nitrogen doping, photocatalytic activity in a broad visible light range was observed with a good efficiency for the degradation of methylene blue by nitrogen doped NiTiO₃ thin films.

1. Introduction

25 Development of visible light driven photocatalysts has been of great interest in the past decade because ultra violet (UV) light induced photocatalysis not only needs expensive light sources but also inefficient in exploiting a large spectrum from solar
30 radiation. TiO₂ shows relatively high reactivity and chemical stability under UV light, whose energy exceeds the band gap of 3.3 eV. Several approaches for TiO₂ modification have been employed such as metal (Ag, Fe, V, Au, Pt, Ni, Co, Cu, Nb) -ion implanted TiO₂,^{1,2} non-metal (N, S, C, B, P, I, F) doped TiO₂,^{1,3}
35 and mixed oxides with p-n junction characteristics.⁴ Attempts have also been made to develop new visible-light photocatalysts such as CdS, WO₃, BiVO₄ and Bi₂O₂CO₃.⁵⁻⁹ However, the resulting photocatalysts are deficient in either activity or stability.

40 A suitable high efficiency semiconductor for visible-light-driven photocatalysis should have sufficiently narrow band gap ($E_g < 3.0$ eV) to harvest visible light, but large enough ($E_g > 1.23$ eV) to provide energetic electrons.¹⁰ In this context NiTiO₃ with a band gap of 2.2 eV has recently attracted much attention because of its

45 high photocatalytic activity under UV irradiation and more remarkably under visible light.¹¹⁻¹³ To the best of our knowledge, most published works have been focused on visible-light photocatalysis of pure or metal doped NiTiO₃ nanoparticles, nanorods and nanowires.^{11,12,14} To enhance the visible light
50 absorption in NiTiO₃, non-metal doping can be one of the simple and low cost option. This approach was successfully applied for TiO₂ where nitrogen doping shifts the absorption edge to lower energies and hence increase the visible light absorption.^{3,15}

55 NiTiO₃ is the only ternary phase with ilmenite structure in the NiO-TiO₂ based materials.^{16,17} For NiTiO₃ (ABO₃), cation arrangement along the c-axis occurs as A-B-Vac-B-A-Vac-A-B.... (Vac = Vacancy) as also observed along the plane perpendicular to the c-axis.^{18,19} Moreover, NiTiO₃ fulfills all
60 conditions such as tolerance factor, electro-negativity difference and octahedral factor to adopt a stable ilmenite structure.²⁰ Thus good stability and related features of ilmenite NiTiO₃ contribute to a wide range of applications for this compound such as tribological coating,²¹ pigment,²² photocatalyst,^{11,12,23} catalyst²⁴
65 and gas sensor.²⁵ However, the above properties depend on the synthesis method. So far different methods have been developed to obtain NiTiO₃ nanoparticles and thin films by different wet chemical methods such as polymer pyrolysis,^{19,26} sol-gel dip

coating,^{25,27} stearic acid gel,²⁸ auto-combustion method,²⁴ co-precipitation,^{2,12} solid state methods like molten salt synthesis^{19,29} and aerosol assisted chemical vapor deposition.³⁰

Efficiency of photocatalytic reactions is critically dependent on the imperfections of the crystalline structure. All the chemical methods require metal-organic molecules, solvents and longer time to reach desired composition and most of above studies involve only powders. Reports concerning the characteristics of NiTiO₃ based thin films deposited by physical vapor depositions are generally lacking. Herein we perform for first time the deposition of nitrogen doped NiTiO₃ thin films by radio frequency magnetron co-sputtering using Ti and Ni metal targets under argon and oxygen atmosphere as well as nitrogen for doped films. An achievement of good crystalline structure of the synthesized NiTiO₃ films was realized as well as the nitrogen doping. Exhaustive studies of structural and optical properties were carried out. The photocatalytic activity tested on methylene blue (MB) solutions shows enhanced efficiency in nitrogen doped film compared to un-doped structures.

2. Experimental details

NiTiO₃ thin films were deposited onto fused quartz substrates using Plassys MP 500S multi-target sputtering unit consisting of two 13.56 MHz, 300 W radio frequency (RF) magnetron sources, as schematically shown in figure 1. Double side polished clean 2 cm × 2 cm quartz substrates were introduced into deposition chamber without any pre-cleaning treatment, except removing the dust particles with an air jet. A 2 inch pure Ni (99.99%) and Ti (99.7%) metal targets with a thickness of 4 and 1 mm, respectively were used. Sputtering chamber was evacuated by turbo molecular pump to a base pressure of 5 × 10⁻⁸ mBar. Argon is used as processing gas, oxygen played reactive gas role and nitrogen doping requires defined nitrogen partial pressure in the deposition chamber. Pre-sputtering was carried out at a RF power of 50 W for 5 minutes in the presence of processing gas with closed shutters. The substrate was mounted apart from target at a distance of 100 mm on a rotating disc. Detailed deposition conditions of nitrogen doped and un-doped NiTiO₃ thin films are listed in table 1. Deposition parameters value was chosen from a set of 12 experiments (L₁₂) designed by Plackett-Burman screening design and from preliminary depositions, which is not reported in this work. The as-deposited films were annealed at 1100 °C for 120 minutes with a heating rate of 5 °C/minute in air.

Structural characterization of NiTiO₃ thin films were carried out using PANalytical Empyrean X-Ray Diffractometer operating at 40 kV, 30 mA with CuK_{α1} (λ = 1.5406 Å) and CuK_{α2} (λ = 1.5444 Å) lines in grazing incidence (ω = 0.3°) mode. X-ray diffraction (XRD) patterns were recorded in the scanning range of 20 - 65° with a scan step size of 0.03°. The XRD pattern was analyzed by the Rietveld method with the Fullprof program (version 5.40).^{31,32} Refinement was carried out by considering space group and lattice parameters from Joint Committee on Powder Diffraction

Standards (JCPDS) database for ilmenite (033-0960) and bunsenite (47-1049). The quality of Rietveld refinement was evaluated in terms of weighted profile residual error (R_{wp}) and profile residual factor (R_p). Confocal Raman scattering was performed with T64000 Jobin-Yvon multichannel spectrometer in simple configuration with 1800 lines/mm grating coupled to a CCD detector. The spectra were collected in the backscattering geometry, under microscope (50X objective) using the 514.5 nm wavelength of Ar-Kr laser source with a power of 200 mW. Surface morphology was captured using JEOL JSM-6510LV scanning electron microscopy (SEM) at an operating voltage of 10 kV with a spot size of 30 nm. Composition of all the films were determined using Oxford X-Max energy dispersive analysis of X-ray (EDAX) system attached to a secondary electron microscope with an accelerating voltage of 10 kV.

The chemical states of NiTiO₃ thin film and nitrogen doping value were studied by using X-ray photoelectron spectroscopy (XPS) measurement performed on SSX-100 (Surface Science Instrument Inc.) with monochromatic Al K_α radiation. Binding energies were calibrated relative to the C 1s peak (284.6 eV). Topography images were obtained on an Agilent 5500 atomic force microscopy (AFM) operating in tapping mode in air at room temperature with a silicon AFM probe. Optical properties of NiTiO₃ thin films were recorded using Cary 100 double beam spectrophotometer in the wavelength range of 200-800 nm. Photocatalytic study was performed under visible light using the degradation of MB as the test reaction. The visible light source was a 240 W high-pressure mercury lamp (100 mm long). A quantity of 50 ml MB blue solution with a concentration of 1 × 10⁻⁵ mol/L under continuous magnetic stirring is taken in a glass beaker and the thin film is placed vertically in the container at a distance of 100 mm from the slit of incident light beam. At regular time intervals, a solution is collected in cuvette and analyzed by measuring the absorption at 661 nm (maximum absorption for MB) using an ulice SPID-PCH UV-vis spectrophotometer.

3. Results and discussion

3.1 Structural features

XRD patterns of NiTiO₃ thin films deposited at 200 and 250 W Ti target power with and without nitrogen atmosphere are depicted in figure 2. Fused quartz used as substrate lead to amorphous-like broad diffraction line at lower angle. With 250 W deposition power, all diffraction peaks were matched to JCPDS card no. 033-0960 (trigonal, a = b = 5.03 Å, c = 13.79 Å, V = 301.69 Å³). The diffraction planes (102), (104), (110), (113), (024), (116), (018), (214) and (300) are situated at 24.34°, 33.33°, 35.94°, 41.07°, 49.66°, 54.36°, 57.80°, 62.64° and 64.30°, respectively, reveal single ilmenite phase NiTiO₃ without any secondary phases. Oppositely, in the case of films deposited at 200 W Ti power with or without doping, three diffraction lines (111), (200) and (220) at 37.48°, 43.66° and 62.98°, respectively were observed corresponding to JCPDS card no. 47-1049 (cubic,

$a = 4.178 \text{ \AA}$, $V = 72.93 \text{ \AA}^3$) along with ilmenite phase for bunsenite phase NiO.

The observed, calculated and difference profiles of Rietveld refined XRD pattern of QNTL84A are illustrated in figure 3. Owing to a low signal-to-noise ratio in the diffraction pattern, a limited number of eight refined parameters were used in the refinement process and consist in scale factors, zero-point value, cell constants and two parameters only for the Thompson-Cox-Hastings pseudo-Voigt function.³³ The atomic coordinates and temperature factors were kept fixed. After Rietveld refinement, lattice parameters and volume of unit cell of two phases were determined as $a = b = 5.02 \text{ \AA}$, $c = 13.77 \text{ \AA}$, $V = 301.39 \text{ \AA}^3$ for NiTiO₃ and $a = 4.172 \text{ \AA}$, $V = 72.63 \text{ \AA}^3$ for NiO. Although there are some changes in the lattice parameters and unit cell volume, they are less than 1 %. Changes in the parameters can be attributed to the stress induced by lattice mismatch between the substrate and the film.³⁴ The final R-factors (not corrected for background values) were R_1 (NiTiO₃) = 15.3%, R_1 (NiO) = 23.5%, $R_p = 6.7%$, $R_{wp} = 8.4%$ and $R_{exp} = 6.7%$. The weight fractions deduced from the Rietveld refinement results are 92 (4) % and 8 (1) % for NiTiO₃ and NiO, respectively. This suggests that these films are nickel rich compared to the one deposited at 250 W Ti power. It is obvious from the phase diagram¹⁷ that NiO coexists with NiTiO₃ phase at higher Ni/Ti ratio. However the film deposited at 250 W Ti power with nitrogen doping showed an extra reflection (110) at 27.66° corresponding to rutile phase (TiO₂; JCPDS card 21-1276). As Ti power increased from 200 W to 250 W, preferential orientation on the film changed from [104] to [110] plane. Influence of nitrogen doping on structural features of NiTiO₃ were not noticed probably due to low doping rates.

Figure 4 shows Raman spectra in the wavenumber range of 150 - 900 cm^{-1} for the NiTiO₃ films deposited at 200 and 250 W Ti power and with and without nitrogen doping. In the case of ilmenite structure, 10 Raman active modes ($5A_g + 5E_g$) were observed and assigned to C_{2v}^2 symmetry with R-3 space group.^{26,27,35} These modes are characteristics of NiTiO₃ and confirm the rhombohedral structure in agreement with the reported literature.^{26,27} The peak positions are located at 193.1, 230.5, 247.6, 292.0, 345.5, 395.2, 465.3, 485.2, 609.6 and 706.8 cm^{-1} . According to Baraton *et al.* at least nine Raman active fundamental modes can be observed without any difficulty in good crystalline structure.³⁵ The remaining mode can be unresolved due to low intensity or overlapping with a closer bands. However, we were able to observe all the active modes in all the samples. Though it's low intensity band, the A_g mode at 485.2 cm^{-1} was also observed. The Raman band at 706.8 cm^{-1} is the highest frequency for fundamental mode of ilmenite phase. This mode arises from the vibrational mode of MO₆ octahedra that is the symmetric stretching mode.³⁵ The assignment of the modes to vibration motions was made in agreement with the similar structure of R-3 space group reported by Wang *et al.* for MgTiO₃ structure.³⁶

3.2 Morphology and composition

Surface morphology of NiTiO₃ thin films deposited at 200 and 250 W Ti target power and with nitrogen doping are shown in figure 5. As witnessed from XRD results, orientation of grains changed from round shape to facets along with pores as power of Ti target increases. Average grain size was measured to be 200-250 nm at 200 W Ti power while two different grain size distributions were observed at 250 W. Grains with similar sizes as seen in 200 W Ti power synthesized films coexist with greater grains up to 500 nm. The atomic concentrations of the investigated films obtained from EDAX are presented in table 2. Increasing Ti target power from 200 to 250 W contributes to lower the ratio of Ni/Ti from 1.7 to 1.2, approaching then the stoichiometry. It's worth noting that EDAX spectrum (figure 6) was not able to evaluate the nitrogen content due to the low doping values as well as the oxygen content due to overlapping of energy lines of Ti $L\alpha$ (0.452 keV) and O $K\alpha$ (0.525 keV). On the hand, Ni/Ti ratio is of primary importance to define the stoichiometry of the films.

The XPS analysis of NiTiO₃ thin film deposited at 250W Ti target power with nitrogen doping (QNTN86A) has been surveyed in the 0-1200 eV range of binding energies as shown in figure 7(a). No contamination species were observed within the sensitivity of the instrument, apart from the adsorbed atmospheric carbon and silicon from the substrate. Peaks corresponding to Ni, Ti and O exist in the sample and nitrogen peak was missing from the spectrum probably because of lower doping levels. The high resolution XPS spectrum of Ni 2p, O 1s and Ti 2p are shown in figure 7(b), (c) and (d), respectively. The peaks in figure 7(b) located at 856 and 874 eV corresponds to the Ni 2p_{3/2} and Ni 2p_{1/2} states.^{14, 37} The broad satellite peaks at 862 eV and 882 eV are characteristic of divalent Ni (Ni²⁺).²⁷ The position of Ti 2p_{3/2} and Ti 2p_{1/2} lines at 458.6 eV and 464.2 eV shown in figure 7(d) indicates to Ti⁴⁺ oxidation state.^{3,37} As shown in figure 7(c), the peak at about 530.3 eV of O 1s can be attributed to NiTiO₃ while the high energy peak at 532.6 eV corresponds to the surface contaminations.³ Atomic concentration of Ni, Ti and O from XPS analysis were 12.06, 12.20 and 75.74 at.%, respectively showing Ni/Ti ratio as 0.99. Ti excess compared to the Ni is the source for rutile phase observed in this film as presented in figure 2. However stoichiometric composition was not extracted from the sample because of signals coming from contamination and the substrate.

Figure 8 shows surface topography of nitrogen doped and undoped NiTiO₃ thin films deposited at 200 and 250 W Ti target power under nitrogen atmosphere. The rms roughness was evaluated as 16.9 nm (QNTN84A) and 19.6 nm (QNTN86A) for the films deposited with nitrogen doping and 12.2 nm (QNTL84A) and 21.0 nm (QNTL86A) for the films deposited without doping. The difference in the surface roughness was observed in all the films and seems to be due to the deposition conditions which monitor drastically the film features. This fact was also noticed for the grain size variation with the increase in Ti target power or under nitrogen partial pressure required for doping. AFM images shown in figure 8 indicate dense, uniform films with columnar grown morphology along c-axis.

3.3 Optical and electronic features

Figure 9 illustrates the absorption properties of NiTiO₃ thin films in the spectral range (200–800 nm). Films deposited at 200 W Ti power show three absorption edges; one at lower wavelength region at about 300 nm (~ 4 eV) related to NiO inter-bands transition indicating the presence of NiO in the sample as noticed from XRD results. Suppression of this band edge occurs in the 250 W grown films which are free from NiO content. The second absorption edge is located at around 400 nm (~ 3 eV) related to direct electronic transition between the upper edge of O 2p valence band and the lower edge of Ti 3d conduction band. Finally a broad absorption edge appeared in the visible region near 600 nm according to the light yellow colored NiTiO₃ film.¹⁴ An inset in figure 9 shows pale yellow color of post-annealed film deposited at 200 W Ti power without nitrogen doping. This indicates that these films indeed absorb visible light in agreement with optical band gap in pure NiTiO₃. With nitrogen doping, slight red shift occurs on the optical absorption spectrum indicating that these films have better visible light response to the ones without doping.

According to Agui and Mizumaki, who studied the intermetallic charge transfer and band gap of MTiO₃ (M = Fe, Mn, Co and Ni), three types of electronic transitions exist in NiTiO₃.³⁸ They are represented as O 2p → Ti 3d, Ni 3d → Ti 3d and Ni 3d → O 2p. Here also two significant absorption edges can be observed due to the crystal field splitting of defined NiTiO₃ bands. Indeed, the one associated with Ni²⁺ that the 3d⁸ ions contributes to splitting of two sub-bands which can be called Ni²⁺ → Ti⁴⁺ charge transfer bands. The second broad absorption edge at shorter wave length is attributed to the O²⁻ → Ti⁴⁺ charge-transfer interactions.^{14,39} In order to obtain optical band gap of NiTiO₃ thin films, the absorbance spectra were fitted by using Tauc's equation given as $(\alpha h\nu)^p = A(h\nu - E_g)$, where A is proportionality constant. From the absorption spectra and the Tauc's equation, the results plotted in figure 10, leads to an evaluation of the band gaps.

The largest band gap for the four investigated samples is related to the direct electronic transition between the upper edge of O 2p valence band and the lower edge of Ti 3d conduction band. The calculated values at 3.16, 3.14, 2.96 and 2.92 eV for QNTL84A, QNTN84A, QNTL86A and QNTN86A respectively, are close to those of TiO₂ structures.⁴⁰ The lower energy occurs from indirect transitions due to correlated electron states in the band gap, which could correspond to Ni²⁺ 3d⁸ band.³⁹ Therefore, the visible light response in the NiTiO₃ films would be due to the transition between the Ni²⁺ 3d⁸ band and Ti⁴⁺ 3d conduction band. The band gap values for these indirect transitions are around 2.65, 2.63, 2.50 and 2.43 eV for QNTL84A, QNTN84A, QNTL86A and QNTN86A as shown in figure 10. According to Zhao *et al.* nitrogen doping in TiO₂ induces two characteristics deep levels resulting band gaps of 1.0 eV and 2.5 eV due to oxygen vacancy and acceptor state of N 2p impurity, respectively.³ The acceptor state is located at the top of the valence band and responsible for reduction in the band gap of nitrogen doped TiO₂. Similarly we noticed a slight drop in the optical band gap of NiTiO₃ films doped with nitrogen and this should improve the visible light

photocatalytic activity.

3.4 Photocatalytic Investigations

Photocatalytic process is based on the photo-generated electron/hole pairs, which can give rise to redox reactions with molecular species adsorbed on the surface of the catalysts. In this frame, photodegradation of methylene blue (MB) solutions was performed on the nitrogen doped and un-doped NiTiO₃ thin films under visible light irradiation. Figure 11 shows the evolution of absorbance of MB versus wavelength with respect to the irradiation time. As shown in figure 11, the rapid decrease in the band intensity at 661 nm for QNTL86A compared to blank solution suggests that the chromophore responsible for characteristic color of MB is mineralized as the irradiation time increases. The change in the solution during photocatalysis reaction is illustrated in the inset of figure 11. No blue shift was observed for the absorption at 661 nm, but a gradual decrease in the absorption intensity was noticed, indicating that the large conjugated π -system has been destroyed.¹¹ We may note however, that a shoulder around 610 nm in MB solution was previously reported as a consequence of MB monomer and dimer formations during the reaction.¹³

Figure 12(a) shows the decrease in relative concentration of MB under visible light irradiation with time. For comparison, MB photolysis without any catalyst (blank solution) was also performed and plotted along with the degradation results. This proves that the decolorization of the MB solution is actually due to the photocatalytic decomposition of the dyes and the extent of decomposition achieved was 60% (figure 12(b)) for the sample deposited at 250 W Ti power without nitrogen doping. A slight increase in the photocatalytic efficiency was observed for the sample deposited at 250 W Ti power with nitrogen doping. The pseudo first order rate constant (k) values related to NiTiO₃ photocatalytic reaction is given by the following equation in terms of logarithmic ratio of MB concentration at time t (C) and at initial time (C₀).^{2,4}

$$-\ln(C/C_0) = kt \quad (1)$$

The k values for NiTiO₃ thin films deposited at 250 W Ti power with (QNTN86A) and without (QNTL86A) nitrogen doping were estimated to be 5.83×10^{-3} and 5.75×10^{-3} /minutes, respectively from the slopes of straight line obtained by plotting $-\ln(C/C_0)$ versus irradiation time as shown in figure 12(c). The initial degradation rate of MB over these films decreased with nitrogen doping and better photocatalytic activity was observed with film doped with nitrogen. Figure 12(d) shows surface topography of the NiTiO₃ thin film deposited at 250 W Ti target power (QNTL86A) after photocatalytic reaction. Rms roughness of the film decreased from 21 to 16.6 nm after 150 minutes of reaction. It can be noticed that the used films as photocatalysts are suitable for re-cycling.

Enhanced visible light photocatalytic activity of nitrogen doped TiO₂ films were reported earlier by Zhao *et al.* and the degradation efficiency on MB solution is given as 47.2 %.³ Y. J. Lin reported photo-degradation of MB on NiTiO₃ powders doped with Ag under visible light irradiation and the time taken for similar degradation efficiency reported in that study is about 60 hours.¹³ X. Shu *et al.* achieved degradation efficiencies of 63 and 73 % for NiTiO₃ and TiO₂ coupled NiTiO₃ nanoparticles, respectively after 6 hours of irradiation under visible light,¹² whereas we report almost equal efficiencies within 2.5 hours. Though the efficiencies obtained in our work are comparable with former reports, the kinetics of the reactions is characterized by shorter times. Thus effective photocatalytic degradation efficiency can be achieved easily (no further purification of the degraded solution is required) by pure NiTiO₃ thin films deposited on quartz substrates at 250 W Ti power. We obtained suitable characteristics of deposited films to act as efficient photocatalyst. For instance structural order is important to achieve crystalline films with defined optical characteristics. This optical band gap is crucial in the photoactivity of films under visible light irradiation and the nitrogen doping enhances the absorbance of these films in visible range contributing then to more efficient photocatalysts.

Conclusions

From the performed work, we demonstrate that pure ilmenite phase NiTiO₃ thin films with nitrogen doping can be grown on quartz substrate, thanks to co-sputtering process using multiple metal targets under partial pressure of oxygen and nitrogen atmosphere. XRD patterns under grazing incidence and well resolved Raman modes revealed high quality of the crystalline structure in investigated films. Formation of facets with porous structure was observed by SEM and AFM on films deposited at higher RF-sputtering power for the titanium target. XPS analysis determined the chemical bonding involved between the constitutive elements and their valence states. Effective effect of nitrogen doping consists in a reduction of the optical band gap of NiTiO₃ films and enhanced absorption in the visible light range. Improvement of the visible light driven photocatalytic activity was achieved from the degradation of MB by nitrogen doped NiTiO₃ thin film. The observed photocatalytic efficiency was attributed to synergetic effects of electronic structure modification induced by nitrogen doping combined with thin film morphology where higher specific surface and porous structure are involved. Potential exploitation is inferred from this work about the relevance of nitrogen doped NiTiO₃ as alternative to TiO₂ based heterogeneous photocatalysts.

Acknowledgements

The authors would like to thank Dr. Nadia Haneche (IMMM) for SEM imaging. Special thanks to Prof. A. Gibaud and Prof. A. Bulou for helpful discussion on XRD and Raman measurements, respectively.

Notes

- ^aInstitute of Molecules and Materials, UMR-CNRS 6283, University of Maine, Avenue O. Messiaen, F-72085 Le Mans, France. Fax: +33 (0)243833518; Tel.: +33 (0)243833512; Email: kassiba@univ-lemans.fr;
- ^bDepartment of Electrical Engineering-SEES, CINVESTAV-IPN, Zacatenco, D.F., C.P. 07360, Mexico.
- ^cA. Chelkowski Institute of Physics and Silesian Centre of Education and Interdisciplinary Research - University of Silesia, Ul. Uniwersytecka 4, 40-007 Katowice, Poland.

References

- 1 A. Zaleska, *Recent patents on Engineering*, 2008, **2**, 157.
- 2 I. Ganesh, A. K. Gupta, P. P. Kumar, P. S. C. Sekhar, K. Radha, G. Padmanabham and G. Sundararajan, *The Scientific World Journal*, 2012, DOI:10.1100/2012/127326, 1.
- 3 L. Zhao, Q. Jiang and J. Lian, *Appl. Surf. Sci.*, 2008, **254**, 4620.
- 4 (a) T. Sreethawong, S. Ngamsinlapasathian and S. Yoshikawa, *Chem. Eng. J.*, 2012, **192**, 292; (b) D. Li, Y. Zhang, W. Wu and C. Pan, *RSC Adv.*, 2014, **4** 18186.
- 5 G. C. De, A. M. Roy and S. S. Bhattacharya, *Int. J. Hydrogen Energy*, 1996, **21**, 19.
- 6 D. W. Hwang, J. Kim, T. J. Park and J. S. Lee, *Catal. Lett.*, 2002, **80**, 53.
- 7 S. D. Scott, J. H. Richard and S. S. Kenneth, *J. Phys. Chem. C*, 2009, **113**, 11980.
- 8 R. Venkatesan, S. Velumani and A. Kassiba, *Mater. Chem. Phys.*, 2012, **135**, 842.
- 9 P. Madhusudan, J. Zhang, B. Cheng and G. Liu, *CrystEngComm*, 2013, **15**, 231.
- 10 Y. Qu, W. Zhou, L. Jiang and H. Fu, *RSC Adv.*, 2013, **3**, 18305.
- 11 X. Shu, J. He, D. Chen and Y. Wang, *J. Phys. Chem. C*, 2008, **112**, 4151.
- 12 X. Shu, J. He and D. Chen, *Ind. Eng. Chem. Res.*, 2008, **47**, 4750.
- 13 Y. J. Lin, Y. H. Chang, G. J. Chen, Y. S. Chang and Y. C. Chang, *J. Alloy. and Compd.*, 2009, **479**, 785.
- 14 (a) Y. Qu, W. Zhou, Z. Ren, S. Du, X. Meng, G. Tian, K. Pan, G. Wang and H. Fu, *J. Mater. Chem.*, 2012, **22**, 16471; (b) P. Jing, W. Lan, Q. Su, M. Yu and E. Xie, *Sci. Adv. Mater.*, 2014, **6**, 1.
- 15 (a) S. S. Soni, M. J. Henderson, J. F. Bardeau and A. Gibaud, *Adv. Mater.*, 2008, **20**, 1493. (b) L. Gomathi Devi and R. Kavitha, *RSC Adv.*, 2014, **4**, 28265.
- 16 K. T. Jacob, V. S. Saji and S. N. S. Reddy, *J. Chem. Thermodynamics*, 2007, **39**, 230.
- 17 A. T. Qiu, L. J. Liu, W. Pang, X. G. Lu and C. H. Li, *Trans. Nonferrous Met. Soc. China*, 2011, **21**, 1808.
- 18 M. Ohgaki, K. Tanaka, F. Marumo and H. Takei, *Mineralogical Journal*, 1988, **14**, 133.
- 19 S. Yuvaraj, V. D. Nithya, K. S. Fathima, C. Sanjeeviraja, G. Kalai Selvan, S. Arumugam and R. Kalai Selvan, *Mater. Res. Bull.*, 2013, **48**, 1110.

- 20 X. C. Liu, R. Hong and C. Tian, *J. Mater. Sci.: Mater. Electron*, 2009, **20**, 323.
- 21 D. J. Taylor, P. F. Fleig, S. T. Schwab and R. A. Page, *Surf. Coat. Tech.*, 1999, **120**, 465.
- 5 22 J. L. Wang, Y. Q. Li, Y. J. Byon, S. G. Mei and G. L. Zhang, *Powder Technol.*, 2013, **235**, 303. 70
- 23 M. Kharkwal, S. Uma and R. Nagarajan, *Ind. Eng. Chem. Res.*, 2010, **49**, 1995.
- 24 G. A. Traistaru, C. I. Covaliu, V. Matei, D. Cursaru and I. Jitaru, *Digest J. Nanomater. Biostructures*, 2011, **6**, 1257.
- 10 25 E. D. Gaspera, M. Pujatti, M. Guglielmi, M. L. Post and A. Martucci, *Mater. Sci. Eng. B*, 2011, **176**, 716. 75
- 26 K. P. Lopes, L. S. Cavalcante, A. Z. Simoes, J. A. Varela, E. Longo and E. R. Leite, *J. Alloy. and Compd.*, 2009, **468**, 327.
- 15 27 S. H. Chuang, M. L. Hsieh, S. C. Wu, H. C. Lin, T. S. Chao and T. H. Hou, *J. Am. Ceram. Soc.*, 2011, **94**, 250.
- 28 M. S. Sadjadi, K. Zare, S. Khanahmadzadeh and M. Enhessari, *Mater. Lett.*, 2008, **62**, 3679. 80
- 29 T. Li, C. C. Wang, C. M. Lei, X. H. Sun, G. J. Wang and L. N. Liu, *Current Applied Physics*, 2013, **13**, 1728.
- 20 30 A. A. Tahir, M. Mazhar, M. Hamid, K. G. U. Wijayantha and K. C. Molloy, *Dalton Trans.*, 2009, 3674.
- 31 H. M. Rietveld, *J. Appl. Crystallogr.*, 1969, **2**, 65. 85
- 32 J. Rodriguez-Carvajal, *J. Physica B*, 1993, **192**, 55.
- 25 33 P. Thompson, D. E. Cox, J. B. Hastings, *J. Appl. Crystallogr.*, 1987, **20**, 79.
- 34 M. M. Shirolkar, D. Phase, V. Sathe, J. Rodriguez-Carvajal, R. J. Choudhary and S. K. Kulkarni, *J. Appl. Phys.*, 2011, **109**, 123512.
- 35 (a) M. I. Baraton, G. Busca, M. C. Prieto, G. Ricciardi and V. Sanchez Escribano, *J. Solid State Chem*, 1994, **112**, 9; (b) G. Busca, 90
- 30 G. Ramis, J. M. Gallardo Amores, V. Sanchez Escribano and P. Piaggio, *J. Chem. Soc. Faraday Trans.*, 1994, **90**, 3181.
- 36 C. H. Wang, X. P. Jing, W. Feng and J. Lu, *J. Appl Phys.*, 2008, **104**, 034112.
- 35 37 G. Yang, W. Chang and W. Yan, *J. Sol-Gel Sci Technol.*, 2014, **69**, 473. 95
- 38 A. Agui and M. Mizumaki, *J. Electron. Spectrosc. Relat. Phenom.*, 2011, **184**, 463.
- 39 S. Moghimiinia, H. Farsi and H. Raissi, *Electrochim. Acta*, 2014, **132**, 512. 40
- 40 M. Landmann, E. Rauls and W. G. Schmidt, *J. Phys. Condensed Matter*, 2012, **24**, 195503. 100

45 105

50 110

55 115

60 120

65

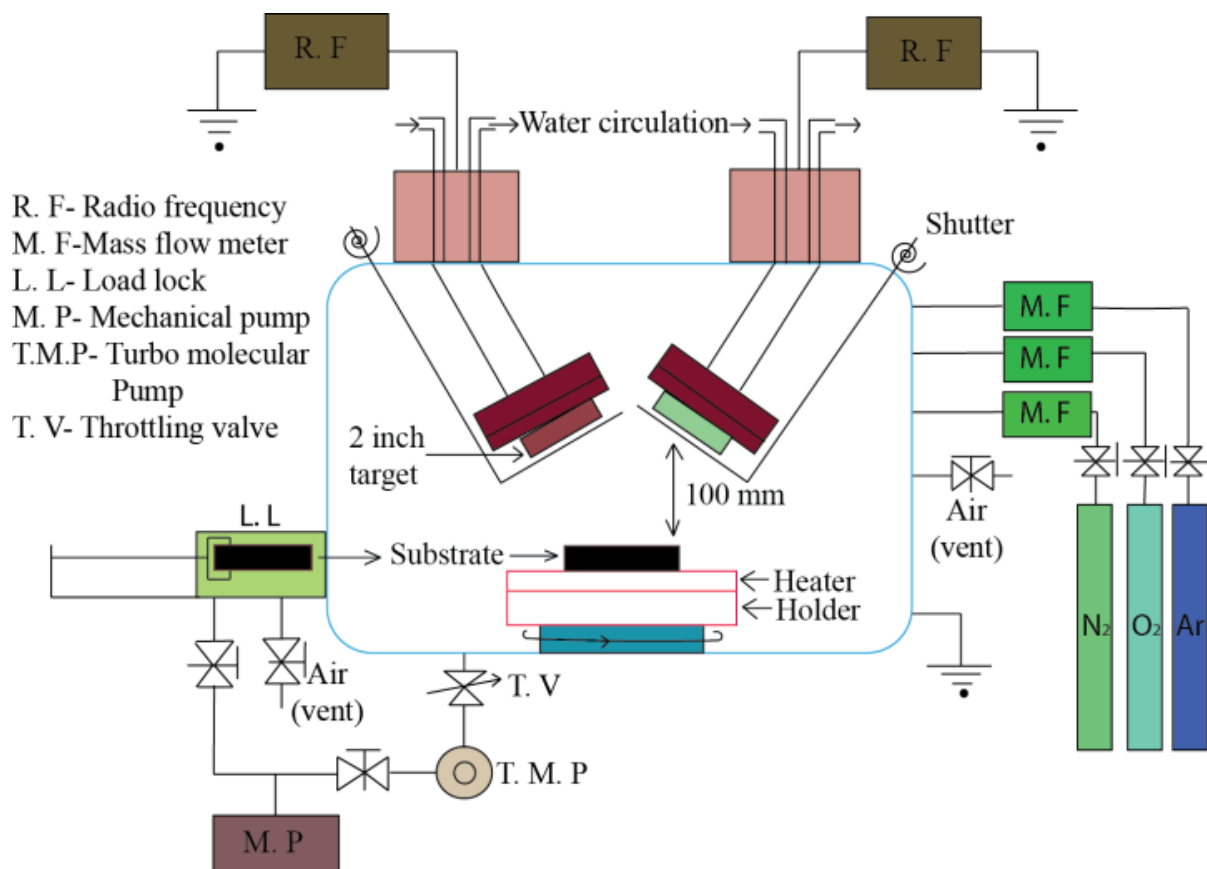


Figure 1 Schematic of two target sputtering system.

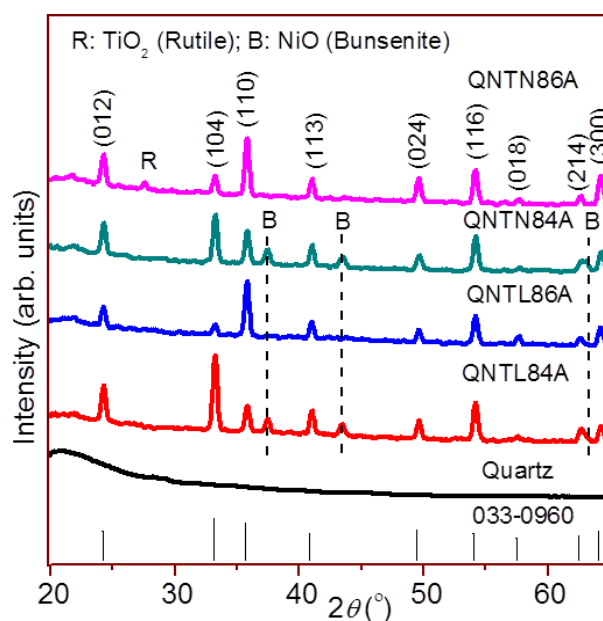


Figure 2 XRD patterns of NiTiO₃ thin films deposited at different Ti power (200 W (QNTL84A) and 250 W (QNTL86A)) with nitrogen doping (QNTN84A and QNTN86A).

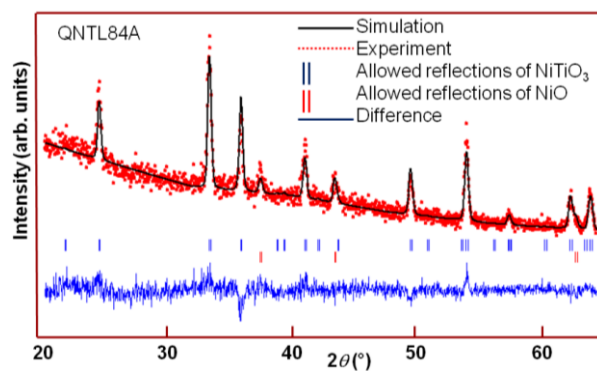


Figure 3 Rietveld refinement for XRD pattern of NiTiO₃ thin film deposited at 200 W Ti power using FullProf software.

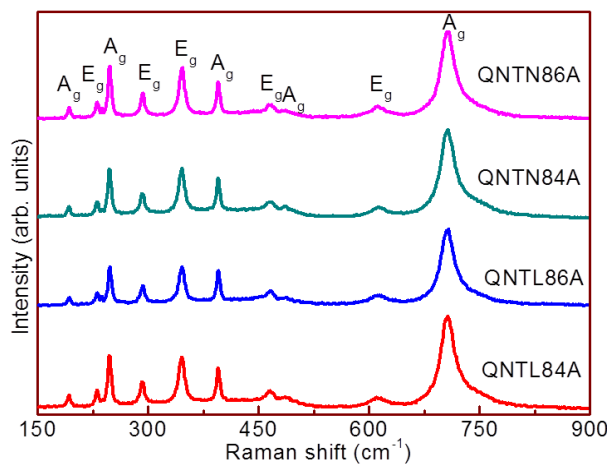


Figure 4 Raman spectra of NiTiO₃ thin films deposited at different Ti power (200 W (QNTL84A) and 250 W (QNTL86A)) with nitrogen doping (QNTN84A and QNTN86A).

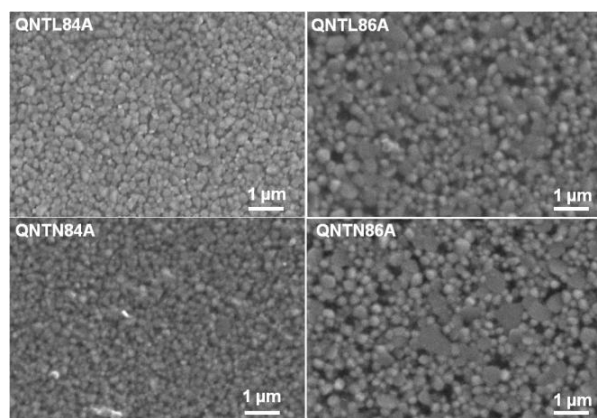


Figure 5 SEM micrographs of NiTiO₃ thin films deposited at 200 and 250 W Ti power with nitrogen doping.

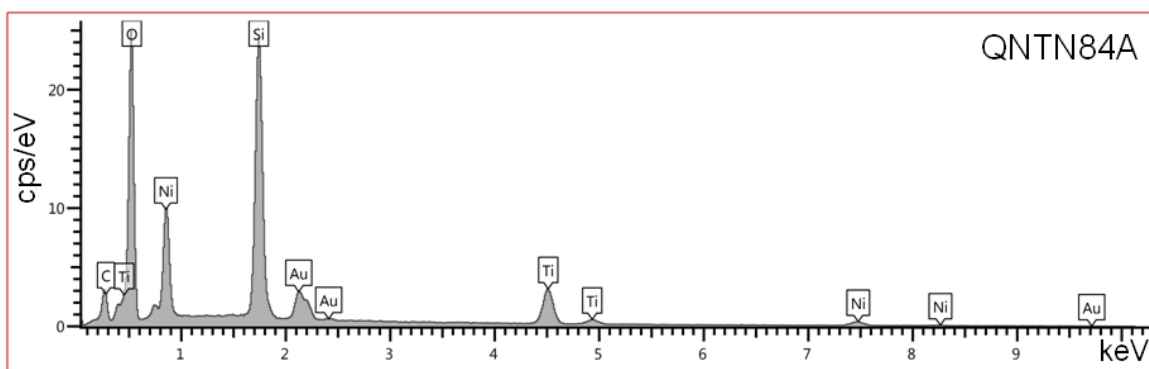


Figure 6 EDAX spectrum of NiTiO₃ thin film deposited at 200 W Ti power with nitrogen doping.

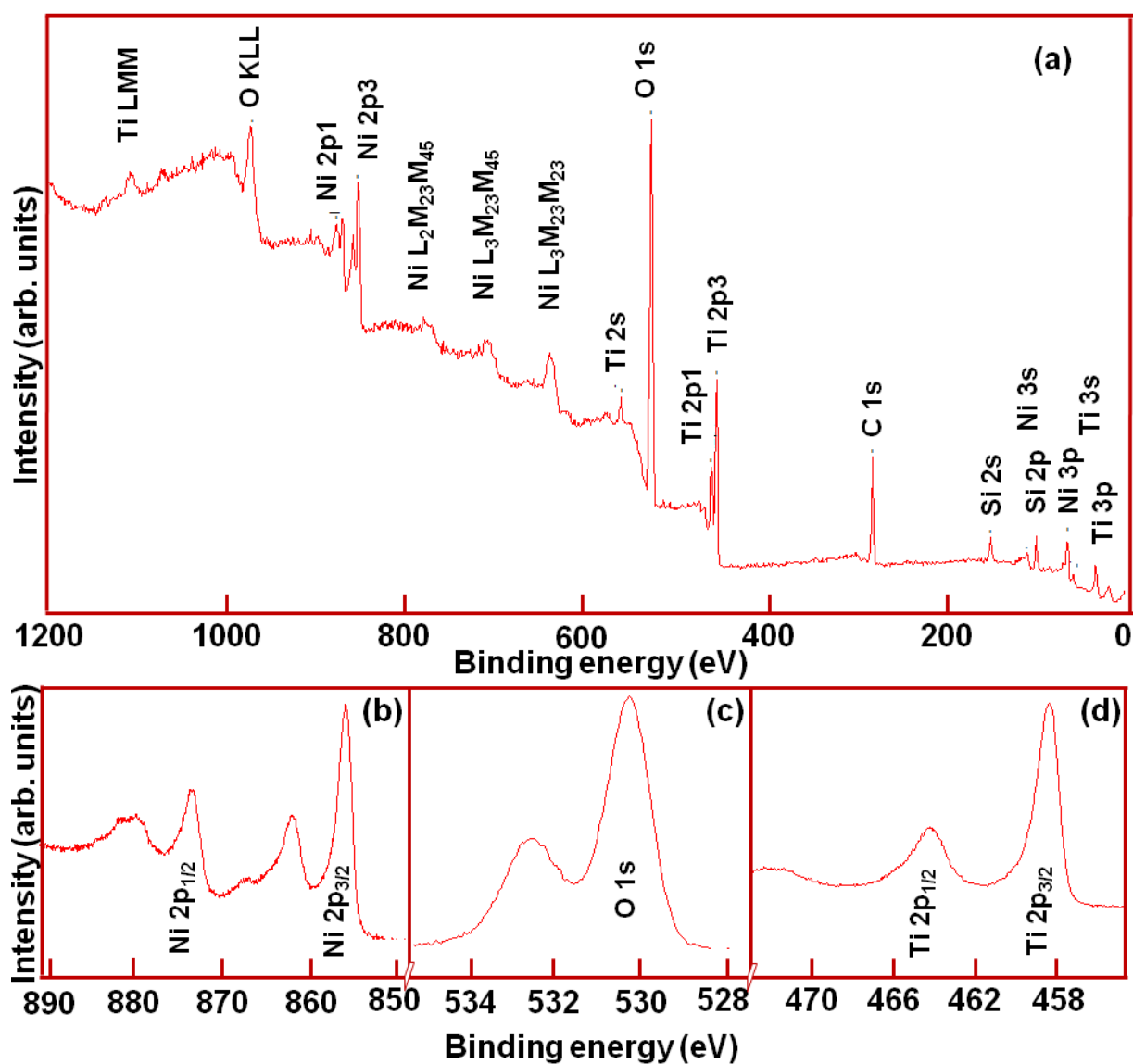


Figure 7 a) XPS survey spectrum of NiTiO₃ thin film deposited at 250 W Ti target power with nitrogen doping (QNTN86A); high resolution XPS spectrum for (b) Ni 2p, (c) O 1s and (d) Ti 2p regions.

5

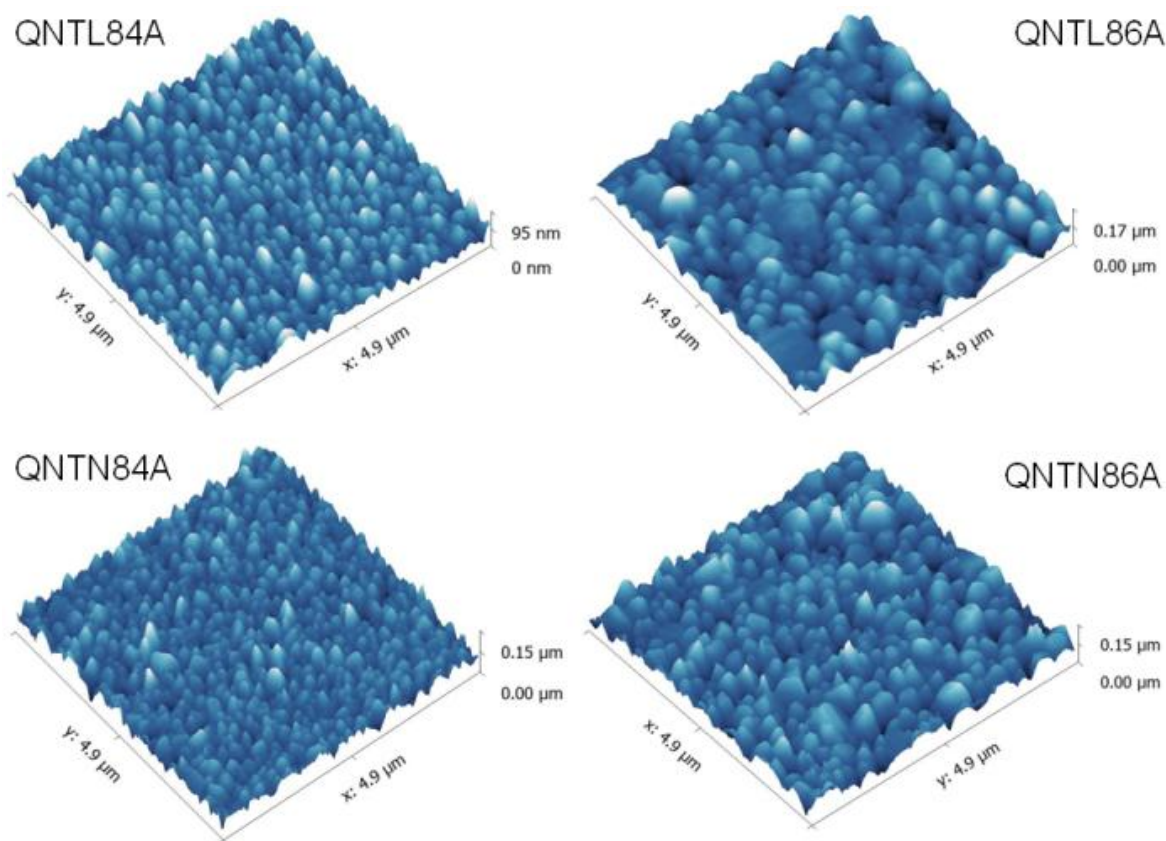


Figure 8 AFM images of NiTiO₃ thin films deposited at 200 and 250 W Ti power with nitrogen doping.

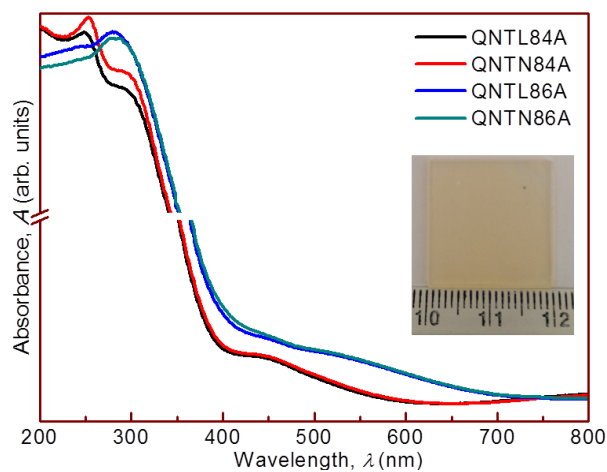


Figure 9 Absorption spectra of NiTiO₃ thin films deposited at different Ti power (200 W (QNTL84A) and 250 W (QNTL86A)) with nitrogen doping (QNTN84A and QNTN86A). An inset shows post-annealed film deposited at 200 W Ti power without nitrogen doping.

5

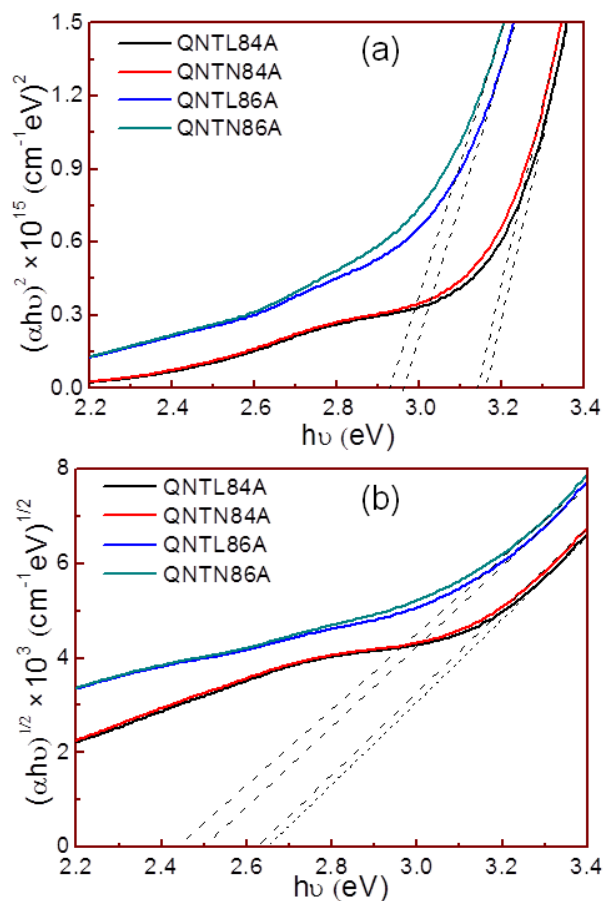


Figure 10 Transformed absorption spectra of NiTiO₃ thin films deposited at different Ti power (200 W (QNTL84A) and 250 W (QNTL86A)) with nitrogen doping (QNTN84A and QNTN86A) showing a) direct and b) indirect band gap energies.

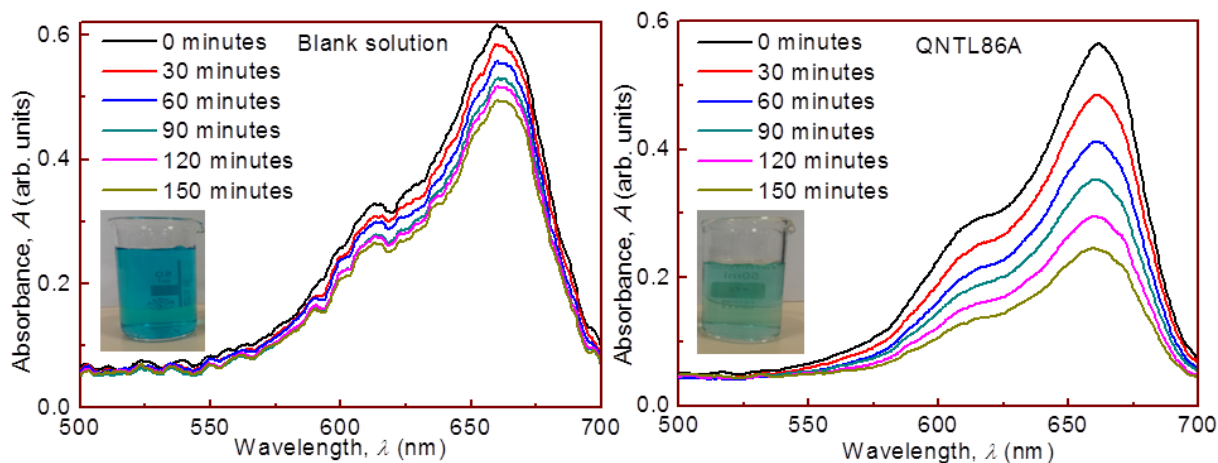


Figure 11 Absorption changes of MB solution on blank (without sample) and NiTiO₃ thin films deposited at 250 W Ti power without nitrogen doping. A photograph of MB solution in the inset shows the de-colorization of the solution before and after the reaction.

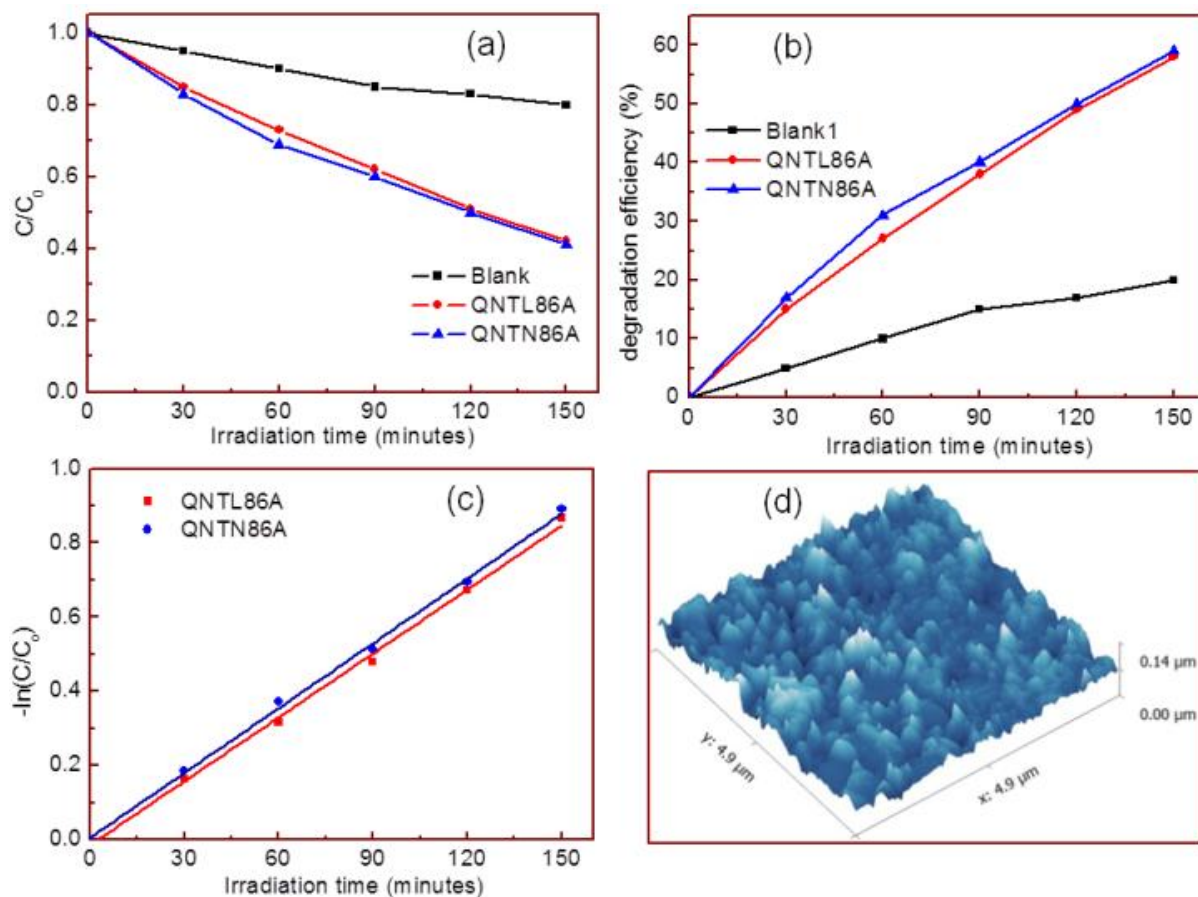


Figure 12 (a) Photodegradation of MB monitored as the normalized concentration change, (b) de-colorization percentage, (c) linear transforms $-\ln(C/C_0)$ versus irradiation time under visible light irradiation for NiTiO₃ thin films deposited at 250 W Ti power (QNTL86A) and with nitrogen doping (QNTN86A) and (d) AFM image of QNTL86A after photocatalytic reaction.

5

Table 1 RF co-sputtering conditions for NiTiO₃ thin films

Deposition parameters	Sample identification			
	QNTL84A	QNTL86A	QNTN84A	QNTN86A
Power of Ni target (W)	40	40	40	40
Power of Ti target (W)	200	250	200	250
Deposition time (minutes)	120	120	120	120
Argon flow rate (sccm)	60	60	60	60
Oxygen flow rate (sccm)	10	10	10	10
Nitrogen flow rate (sccm)	---	---	2	2
Substrate temperature (°C)	400	400	400	400
Working pressure (mBar)	0.02	0.02	0.02	0.02
Annealing temperature (°C)	1100	1100	1100	1100
Annealing time (minutes)	120	120	120	120

Table 2 EDAX analysis of NiTiO₃ thin films

Sample identification	Atomic concentration of		
	Ni (at. %)	Ti (at. %)	O (at. %)
QNTL84A	17.36	10.24	72.39
QNTL86A	15.02	12.39	72.59
QNTN84A	17.33	10.20	72.47
QNTN86A	15.13	12.12	72.76

5